THE JOURNAL OF BIOLOGICAL CHEMISTRY VOL. 285, NO. 44, pp. 34279–34287, October 29, 2010

Crystal Structures of Phosphoketolase

THIAMINE DIPHOSPHATE-DEPENDENT DEHYDRATION MECHANISM[*S]

Received for publication, June 19, 2010, and in revised form, August 13, 2010 Published, JBC Papers in Press, August 24, 2010, DOI 10.1074/jbc.M110.156281

Ryuichiro Suzuki[‡1], Takane Katayama[§], Byung-Jun Kim[¶], Takayoshi Wakagi[‡], Hirofumi Shoun[‡], Hisashi Ashida[¶], Kenji Yamamoto[¶], and Shinya Fushinobu[‡2]

From the [‡]Department of Biotechnology, The University of Tokyo, 1-1-1 Yayoi, Bunkyo-ku, Tokyo 113-8657, Japan, the [§]Research Institute for Bioresources and Biotechnology, Ishikawa Prefectural University, Nonoichi-cho, Ishikawa 921-8836, Japan, and the [¶]Graduate School of Biostudies, Kyoto University, Kitashirakawa, Sakyo-ku, Kyoto 606-8502, Japan

Thiamine diphosphate (ThDP)-dependent enzymes are ubiquitously present in all organisms and catalyze essential reactions in various metabolic pathways. ThDP-dependent phosphoketolase plays key roles in the central metabolism of heterofermentative bacteria and in the pentose catabolism of various microbes. In particular, bifidobacteria, representatives of beneficial commensal bacteria, have an effective glycolytic pathway called bifid shunt in which 2.5 mol of ATP are produced per glucose. Phosphoketolase catalyzes two steps in the bifid shunt because of its dual-substrate specificity; they are phosphorolytic cleavage of fructose 6-phosphate or xylulose 5-phosphate to produce aldose phosphate, acetyl phosphate, and H_2O. The phosphoketolase reaction is different from other well studied ThDP-dependent enzymes because it involves a dehydration step. Although phosphoketolase was discovered more than 50 years ago, its three-dimensional structure remains unclear. In this study we report the crystal structures of xylulose 5-phosphate/fructose 6-phosphate phosphoketolase from *Bifidobacterium breve*. The structures of the two intermediates before and after dehydration (α,β-dihydroxyethyl ThDP and 2-acetyl-ThDP) and complex with inorganic phosphate give an insight into the mechanism of each step of the enzymatic reaction.

Bifidobacteria represent a ubiquitous commensal bacterial group in the gastrointestinal tract of humans and animals (1). A unique central hexose fermentation pathway of bifidobacteria is called the "bifid shunt," which is summarized in the following scheme (2).

$$2\ \text{glucose} + 5\ P_i + 5\ \text{ADP} \rightarrow 3\ \text{acetate} + 2\ \text{lactate} + 5\ \text{ATP} + 5\ H_2O$$

SCHEME 1

Therefore, ATP production by the bifid shunt is 1.25-fold more effective than that by lactic acid fermentation in the well known Embden-Meyerhof glycolytic pathway (2 ATP per glucose). Two thiamine diphosphate (ThDP)[3]-dependent enzymes, transketolase (TK) and phosphoketolase (PK), catalyze key steps of the bifid shunt (Fig. 1). The structure and mechanism of TK has been extensively studied (3, 4). However, the three-dimensional structure and reaction mechanism of PK has long been enigmatic, although PK was discovered in 1958 (5–7).

ThDP is a biologically active form of vitamin B_1. ThDP-dependent enzymes are ubiquitously present in all organisms and catalyze various essential reactions in metabolic pathways. These enzymes generally catalyze the conversion of 2-keto acid and require ThDP and divalent cations as cofactors. Formation of ThDP ylide, which is accomplished by deprotonation of the C2 atom on the thiazolium ring, is the first essential activation step (Fig. 2) (8, 9). ThDP-dependent enzymes are divided into four families based on their primary and tertiary structures (10). Three of the four families catalyze oxidative decarboxylation reactions to produce biologically essential metabolites such as acetyl-CoA (9, 11, 12). Acetyl phosphate (acetyl-P)-producing pyruvate oxidase (POX), which belongs to one of the oxidative decarboxylation-catalyzing families, cleaves pyruvate in the presence of inorganic phosphate (P_i) and O_2 to produce acetyl-P, CO_2, and H_2O_2 (Fig. 2) (13). TK is a representative member of the fourth family (known as the TK family). The reactions of enzymes belonging to this family are significantly different from those belonging to other families because the TK family enzymes catalyze non-oxidative reactions. TK catalyzes the cleavage of a C-C bond in ketose phosphate (donor substrate) into a two-carbon fragment and aldose phosphate. This cleavage is subsequently followed by condensation of the ThDP-bound two-carbon fragment with aldose (acceptor substrate).

PK belongs to the TK family, and there are two types of enzymes with different preferences for sugar phosphate substrates exist. Xylulose-5-phosphate PK (XPK, EC 4.1.2.9) pre-

* This work was supported by the Program for the Promotion of Basic Research Activities for Innovative Bioscience (PROBRAIN) in Japan.

[S] The on-line version of this article (available at http://www.jbc.org) contains supplemental Tables 1–3 and Figs. 1–5.

The atomic coordinates and structure factors (codes 3AHC, 3AHD, 3AHE, 3AHF, 3AHG, 3AHH, 3AHI, and 3AHJ) have been deposited in the Protein Data Bank, Research Collaboratory for Structural Bioinformatics, Rutgers University, New Brunswick, NJ (http://www.rcsb.org/).

[1] Present address: Applied Microbiology Division, National Food Research Institute, National Agriculture and Food Research Organization, 2-1-12 Kannondai, Tsukuba 305-8642, Japan.

[2] To whom correspondence should be addressed: Dept. of Biotechnology, The University of Tokyo, 1-1-1 Yayoi, Bunkyo-ku, Tokyo 113-8657, Japan. Tel./Fax: 81-3-5841-5151; E-mail: asfushi@mail.ecc.u-tokyo.ac.jp.

[3] The abbreviations used are: ThDP, thiamine diphosphate; TK, transketolase; PK, phosphoketolase; POX, pyruvate oxidase; acetyl-P, acetyl phosphate; XPK, xylulose 5-phosphate phosphoketolase; X5P, xylulose 5-phosphate; F6P, fructose 6-phosphate; XFPK, xylulose 5-phosphate/fructose 6-phosphate phosphoketolase; DHEThDP, α,β-dihydroxyethyl ThDP; AcThDP, 2-acetyl-ThDP; *Bb*XFPK, XFPK from *B. breve*; *Sc*TK, TK from *S. cerevisiae*; *Lp*POX, POX from *L. plantarum*; *Ec*TK, TK from *E. coli*; Bicine, *N*,*N*-bis(2-hydroxyethyl)glycine.

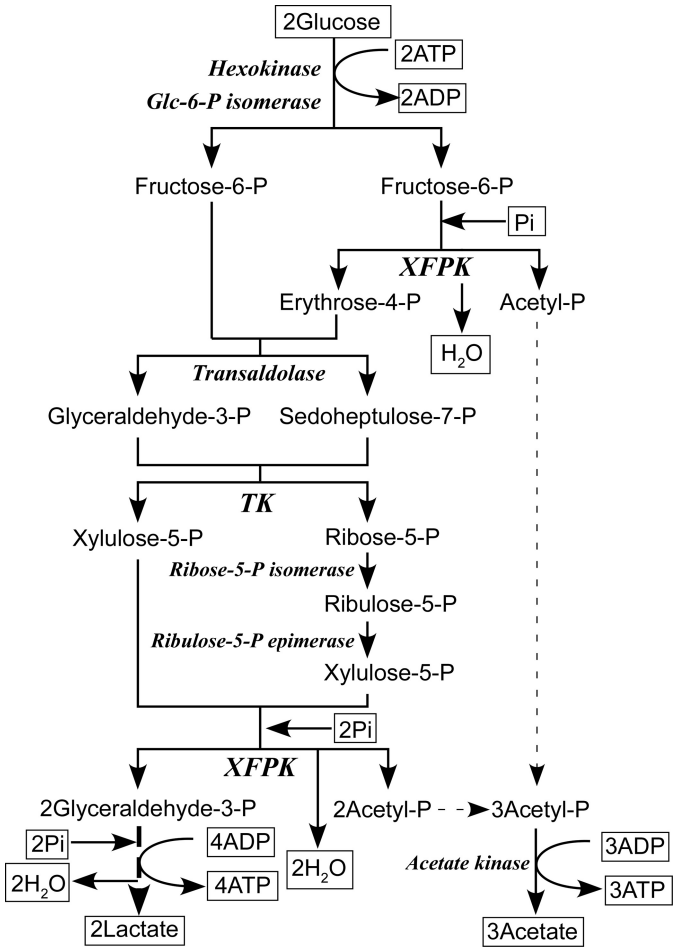

FIGURE 1. **The central metabolism of bifidobacteria, the bifid shunt.** XFPK is involved in two steps of the bifid shunt.

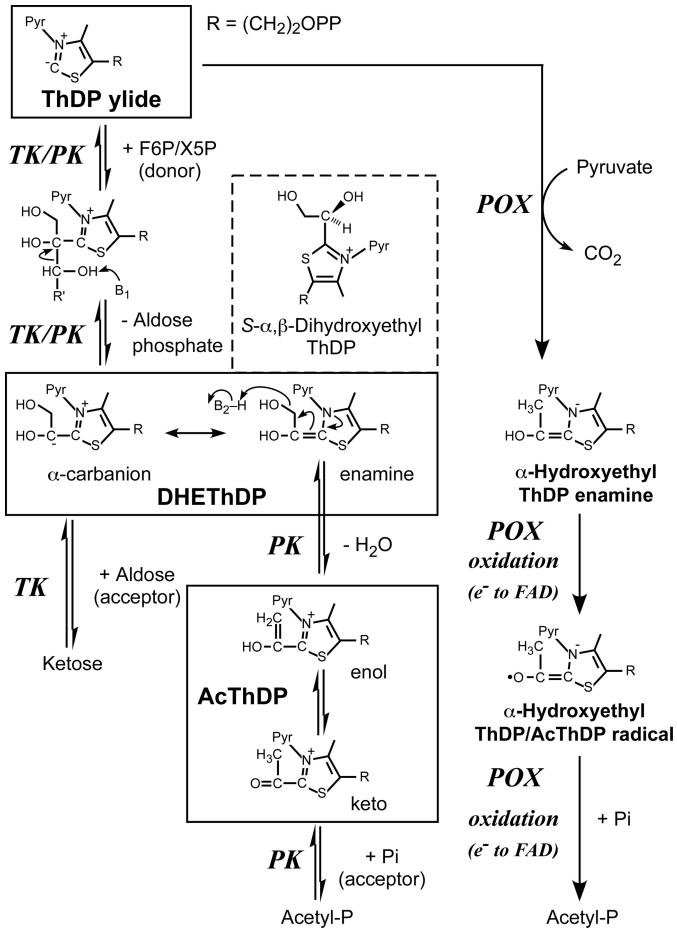

FIGURE 2. **Reaction mechanisms of TK, PK, and acetyl-P-producing POX.** The first-half reactions of XFPK and TK are identical, but the second-half- reactions diverge. The reaction catalyzed by POX involves oxidation and radical chemistry. *Pyr* represents the aminopyrimidine ring of ThDP. Protonated DHEThDP (*S*-α,β-dihydroxyethyl-ThDP), which is likely the state observed in our crystal structure, is also shown.

fers xylulose 5-phosphate (X5P) to fructose 6-phosphate (F6P) (5, 6), whereas X5P/F6P PK (XFPK, EC 4.1.2.22) acts on both X5P and F6P with comparable activities (7, 14–16). These enzymes constitute two homologous (sequence identity > 40%) but phylogenetically distinct groups (supplemental Figs. 1 and 2 and supplemental Table 1) (17). PKs catalyze the cleavage of X5P or F6P (donor) utilizing P_i as the acceptor (phosphorolysis) to produce acetyl-P, water, and glyceraldehyde 3-phosphate or erythrose 4-phosphate.

$$X5P + P_i \rightarrow \text{acetyl-P} + H_2O + \text{glyceraldehyde 3-phosphate (XPK and XFPK)} \quad \text{(Eq. 1)}$$

$$F6P + P_i \rightarrow \text{acetyl-P} + H_2O + \text{erythrose 4-phosphate (XFPK)} \quad \text{(Eq. 2)}$$

The XFPK-type gene has only been found in bifidobacteria, and XFPK catalyzes two steps in the bifid shunt because of its dual-substrate specificity (Fig. 1). Because PK activity against F6P is specific to the bifid shunt, it is employed as the most reliable non-molecular test for identification of bifidobacteria (18, 19).

XPK is a key enzyme in the pentose catabolism in various microbes, including filamentous fungi and yeasts (17). This pentose catabolism is called the "PK pathway" (20). Furthermore, the PK pathway is the central pathway in the metabolism of heterofermentative lactic acid bacteria including the genera *Lactobacillus* and *Leuconostoc*. Heterofermentative lactic acid bacteria, representatives of beneficial gut microbes (probiotics), produce lactic and acetic acids as the main end products. These short-chain fatty acids are important for hosts, not only because they prevent the growth of harmful bacteria by lowering the intestinal pH but also because they serve as an energy source for intestinal epithelial cells. In addition, short-chain fatty acids can modulate intestinal immune and inflammatory responses via G-protein-coupled receptors (21).

Recently, kinetic analysis of PK-2 from *Lactobacillus plantarum*, belonging to the XPK group, revealed that the reaction follows a ping-pong bi-bi mechanism, leading to the proposal that the first-half of the reaction by PK proceeds through the same mechanism as TK and forms an α,β-dihydroxyethyl ThDP (DHEThDP) intermediate (Fig. 2) (22). However, the subsequent reaction catalyzed by PK is distinct from TK at the following two points; 1) the dehydration reaction occurs, and 2) the acceptor substrate P_i is believed to attack the possible 2-acetyl-ThDP (AcThDP) intermediate, similar to the case of acetyl-P-producing POX.

TABLE 1
Data collection and refinement statistics
SAD, single anomalous diffraction; r.m.s.d., root mean square deviation.

Data set	Native resting	Native/AcThDP	Native/DHEThDP	Native/Pi	SAD peak
Data collection statistics					
Space group			I422		
Unit cell (Å)	$a = 174.8$ $b = 174.8$ $c = 163.8$	$a = 174.4$ $b = 174.4$ $c = 163.8$	$a = 173.5$ $b = 173.5$ $c = 163.5$	$a = 173.9$ $b = 173.9$ $c = 163.5$	$a = 174.0$ $b = 174.0$ $c = 163.8$
Beam line	PFAR-NE3A	PF-BL5A	PFAR-NW12A	PF-BL6A	Spring-8 BL38B1
Wavelength (Å)	1.00000	1.00000	1.00000	0.97800	0.97875
Resolution (Å)[a]	50-1.70 (1.73-1.70)	50-1.90 (1.93-1.90)	50-2.10 (2.14-2.10)	50-2.30 (2.38-2.30)	50-2.60 (2.69-2.60)
Total reflections	2,049,689	1,442,105	1,079,159	633,806	575,648
Unique reflections	137,590	98,940	72,417	55,669	38,884
Completeness (%)[a]	100 (100)	99.9 (100)	100 (100)	100 (100)	99.9 (100)
R_{merge} (%)[a]	6.5 (32.2)	7.0 (34.9)	7.1 (29.8)	10.8 (35.5)	6.7 (22.1)
$I/\sigma I$[a]	49.6 (7.4)	52.6 (9.0)	42.8 (11.0)	24.9 (4.7)	32.9 (9.4)
Redundancy[a]	14.9 (14.8)	14.6 (14.7)	14.9 (15.0)	11.4 (10.4)	7.8 (7.7)
Refinement statistics					
Resolution range (Å)	34.18-1.70	34.21-1.90	49.07-2.10	40.88-2.30	
No. of reflections	130,627	93,681	68,524	52,685	
R-factor/R_{free} (%)[b]	15.0/18.1	16.2/19.7	16.1/20.6	17.7/22.6	
r.m.s.d. from ideal					
Bond lengths (Å)	0.037	0.030	0.028	0.023	
Bond angles (°)	2.722	2.212	2.066	1.904	
Average B-factor (Å^2)					
Protein	18.1	22.7	20.9	28.1	
Water	30.2	33.4	32.1	32.6	
ThDP	16.5	18.9	19.1	20.9	
Mg^{2+}	13.2	16.1	15.4	21.2	
Ramachandran plot (%)[c]					
Favored	96.6	96.6	96.1	95.5	
Allowed	3.4	3.4	3.9	4.4	
Outlier	0.0	0.0	0.0	0.1	

[a] Values for highest resolution shell are given in parentheses.
[b] R_{free} actor was calculated using 5% of the unique reflections.
[c] Calculated by RAMPAGE (45).

Recently, preliminary x-ray crystallographic studies of XPK from *Lactococcus lactis* (23) and XFPK from *Bifidobacterium breve* 203 (*Bb*XFPK) (24) are reported. In this study we report the crystal structure of *Bb*XFPK as the first three-dimensional structure of PK. The structures of the resting form, the two intermediates before and after dehydration (DHEThDP and AcThDP), the complex with the acceptor substrate P_i, and four mutant enzymes have been determined. This study revealed a structural basis for the reaction mechanism of a ThDP-dependent enzyme involving dehydration and nucleophilic attack of P_i to the AcThDP intermediate.

EXPERIMENTAL PROCEDURES

Enzyme Preparation and Assay—Construction of the expression vector, protein expression, purification, and kinetic analysis employing F6P as the donor substrate were performed as described previously (24). Mutants of *Bb*XFPK were constructed using a QuikChange site-directed mutagenesis kit (Stratagene, La Jolla, CA) using the primers summarized in supplemental Table 2.

Crystallography—Native (resting) *Bb*XFPK and its mutants were crystallized according to the method described previously (24). Structures of AcThDP intermediate (*Bb*XFPK/AcThDP), DHEThDP intermediate (*Bb*XFPK/DHEThDP), and *Bb*XFPK in complex with the acceptor substrate P_i (*Bb*XFPK/P_i) were trapped using cryocrystallography technique. Crystals of *Bb*XFPK/AcThDP were prepared by soaking native *Bb*XFPK crystals in mother liquor (24% (*v*/*v*) PEG 6000, 0.1 M Bicine buffer, pH 9.0) containing 27 mM F6P for various time periods at room temperature. *Bb*XFPK/DHEThDP crystals were obtained by soaking in 54 mM F6P solution for 15 s. Crystals of *Bb*XFPK/P_i were obtained by cocrystallization with 5 mM potassium phosphate. The mother liquor containing 20% ethylene glycol was used as a cryoprotectant, except for the *Bb*XFPK/P_i complex for which 20% glycerol was used. Selenomethionine-labeled enzyme was expressed in *Escherichia coli* B834 (DE3) (Novagen, Madison, WI). Diffraction data were collected using beamlines at SPring-8 (Harima, Japan) and Photon Factory (Tsukuba, Japan). Diffraction data were processed using HKL2000 (25). Initial phases were calculated using SnB (26) and Solve/Resolve (27). Initial model building was performed using ARP/wARP (28). Manual model rebuilding and refinement was achieved using Coot (29) and REFMAC5 (30). Parameters for refinement were generated by the PRODRG server (31). Details of data collection and refinement statistics are given in Table 1 and supplemental Table 3. Figures were prepared using PyMol (DeLano Scientific, Palo Alto, CA).

RESULTS

Overall Structure—The crystal structures (residues 5–806) of the resting form, the AcThDP intermediate, the DHEThDP intermediate, and the complex with P_i were determined at 1.7, 1.9, 2.1, and 2.3 Å, respectively (Table 1). The dimeric and monomeric structures of *Bb*XFPK are shown in Fig. 3, *A* and *B*. *Bb*XFPK consists of three α/β-fold domains; N-terminal (PP domain, residues 5–378), middle (Pyr domain, residues 379–611), and C-terminal (residues 612–806) domains. The crystals contain one molecule per asymmetric unit, and a crystallographic 2-fold axis is consistent with the molecular axis of the dimer. The active site is positioned at the interface between the

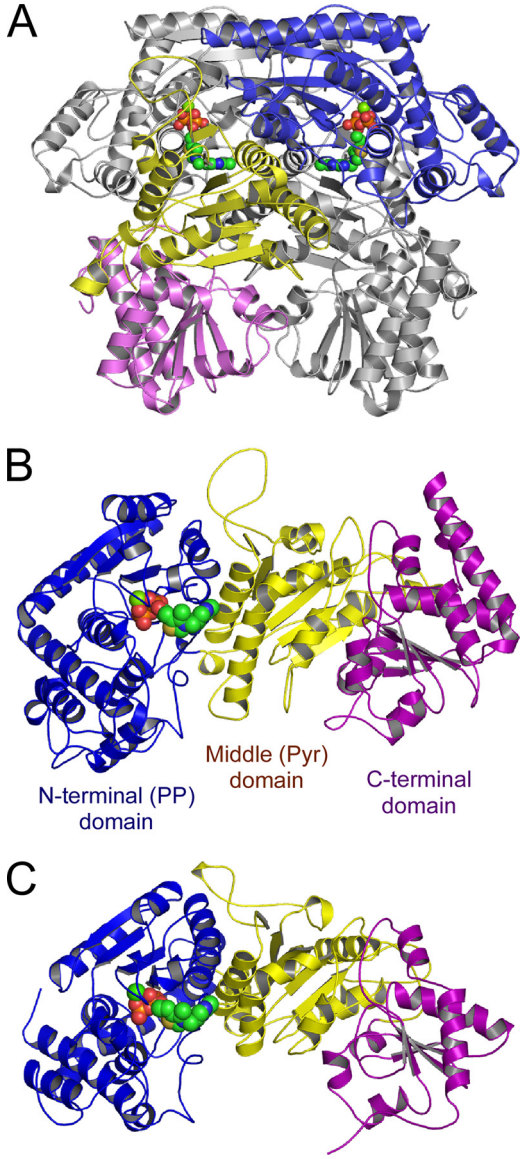

FIGURE 3. **Overall structures of homodimer (*A*) and monomer (*B*) of *Bb*XFPK and the monomer structure of *Sc*TK (*C*).** The N-terminal PP (*blue*), middle Pyr (*yellow*), and C-terminal (*purple*) domains are colored differently. ThDP molecules are shown as *spheres*. *A*, the subunit located at the distant side is shown in *gray*.

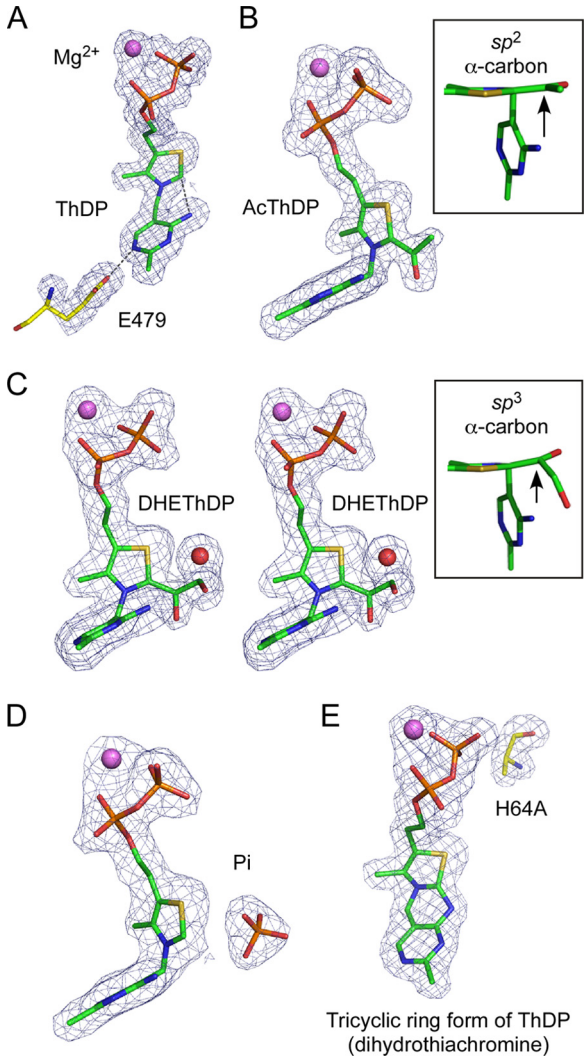

FIGURE 4. **$|F_o| - |F_c|$ omit electron density maps of resting ThDP (*A*), AcThDP (*B*), DHEThDP (*C*), P_i complex (*D*), and tricyclic ring form of ThDP in H64A mutant (*E*).** The maps were contoured at 4σ (*A*, *B*, *D*, and *E*) or 3σ (*C*). *A*, a catalytically important Glu-479 residue is also shown. Interactions between the N4′ group of pyrimidine and the reactive C2 atom of the thiazolium ring and between the N1′ atom of the pyrimidine and Glu479 are shown as *dotted lines*. *B*, the *inset* shows planarity of the acetyl group. *C*, this *panel* is stereographic. The *inset* shows nonplanarity of the DHE moiety. *E*, the mutated Ala-64 residue is also shown.

PP and Pyr domains from different subunits to form a deep and narrow substrate channel, and the reactive C2 atom of ThDP is only accessible from the solvent. These observations suggest that the minimum functional unit of the enzyme is a homodimer. The overall architectures of the monomer and the tightly packed homodimer of *Bb*XFPK are basically similar to those of TK (Fig. 3*C*) (3), with a root mean square deviation of 2.6 Å for 545 α-carbon atoms. However, they share very low sequence homology, with a sequence identity of 15% based on structural alignment with TK from *Saccharomyces cerevisiae* (*Sc*TK). Three active peaks of *Bb*XFPK appeared on gel filtration chromatography with different estimated sizes (24). A sample from the major homohexameric peak successfully crystallized, whereas those from the two minor peaks (homodimer and homotetramer) failed to crystallize. We examined the crystal packing, but there was no strong interaction that possibly interconnects the dimer units (data not shown). The biological assembly might have collapsed under the crystallization condition.

Structures of Resting Form, AcThDP and DHEThDP Intermediates, and the P_i Complex—In all structures determined here, ThDP binds in a typical V-conformation (Fig. 4). The pyrimidine and thiazolium rings are held mainly through the hydrophobic residues of the PP and Pyr domains (supplemental Fig. 3*A*). The diphosphate group of ThDP and the hexacoordinated Mg^{2+} are anchored to the PP domain through many interactions (supplemental Fig. 3*B*). Several histidine residues in the active site as well as other residues important for catalysis are completely conserved between *Bb*XFPK and TK (discussed later).

In the initial reaction step of all ThDP-dependent enzymes, formation of reactive ThDP ylide is achieved by cofactor-as-

TABLE 2
Kinetic parameters for wild-type and mutant *Bb*XFPK

Enzyme	K_{cat}	Apparent K_m		Cofactor in mutant structures[a]
		F6P	P_i	
	min^{-1}	mM		
WT[b]	1,540 ± 60	9.7 ± 0.3	1.2 ± 0.2	
H64A	NA[c]	NA	NA	Tricyclic ring form of ThDP
H64N	NA	NA	NA	
H97A	NA	NA	NA	(CDNG[d])
H97N	NA	NA	NA	(CDNG[d])
H142A	12.2 ± 0.9	7.4 ± 0.6	1.7 ± 0.2	AcThDP
H142N	39.2 ± 1.2	7.2 ± 0.8	2.6 ± 0.5	
H320A	NA	NA	NA	AcThDP
H320N	NA	NA	NA	
Q321A	59.5 ± 2.5	4.4 ± 0.3	1.6 ± 0.2	
S440A	350 ± 11	53.5 ± 1.8	0.57 ± 0.04	
E479A	NA	NA	NA	
Y501F	197 ± 4	1.4 ± 0.2	25.5 ± 1.7	
H548A	100 ± 3	2.3 ± 0.7	0.52 ± 0.16	
N549A	NA	NA	NA	
H553A	NA	NA	NA	ThDP
H553N	NA	NA	NA	
K605A	NA	NA	NA	

[a] Crystallographic data collected after soaking in 27 mM F6P for 5 min. See supplemental Table 3 for details.
[b] The data are taken from (24).
[c] NA, no activity was detected.
[d] CDNG, crystals did not grow.

sisted deprotonation of the C2 atom of the thiazolium ring by the N4′-imino group of the pyrimidine ring, and the imino tautomer is stabilized by a completely conserved Glu residue (9, 32). In the resting structure, interactions between the N4′ atom and the reactive C2 atom (2.9 Å) and between the N1′ atom of pyrimidine and the conserved Glu479 (2.7 Å) residue are present (Fig. 4*A*). Replacement of this residue (E479A) completely abolished the activity (Table 2). These results indicate that the initial activation mechanism of *Bb*XFPK to form ThDP ylide is identical to that of other ThDP-dependent enzymes.

When we collected diffraction data from crystals soaked in 27 mM F6P for 5 min in the absence of P_i, extra electron density was observed (Fig. 4*B*). The density corresponds to three branched carbon or oxygen atoms and is covalently attached to the C2 atom of the thiazolium ring. The appearance of the electron density did not change when the soaking time was varied in a range from 1 to 60 min (data not shown). The central Cα atom appears to be sp^2-hybridized because the map of the covalent adduct is trigonal planar (Fig. 4*B*, *inset*). Based on these observations, we concluded that the covalent adduct is an acetyl group. It has been proposed that AcThDP formed after dehydration is a stable intermediate of PK in the absence of the acceptor, P_i (22, 33). One of the two terminal atoms is located close to the NE2 atom of His-553 (2.5 Å) and the N4′ atom of the pyrimidine ring (3.2 Å) (Fig. 5*A*, *gray*). Superimposition with the *Sc*TK-DHEThDP structure illustrates that this atom overlaps with the Cα hydroxyl group of DHEThDP (Fig. 5*B*), suggesting that it is an oxygen atom. Careful inspection of the heights of electron density peaks and temperature factors supported this assignment of terminal oxygen and carbon atoms. We refined the structure using the parameters of keto-AcThDP. The resolution was not sufficiently high to determine whether it is a keto or an enol form. The planar character of the Cα atom is consistent with the similar AcThDP adduct of *L. plantarum* POX (*Lp*POX) (34). A water molecule is located

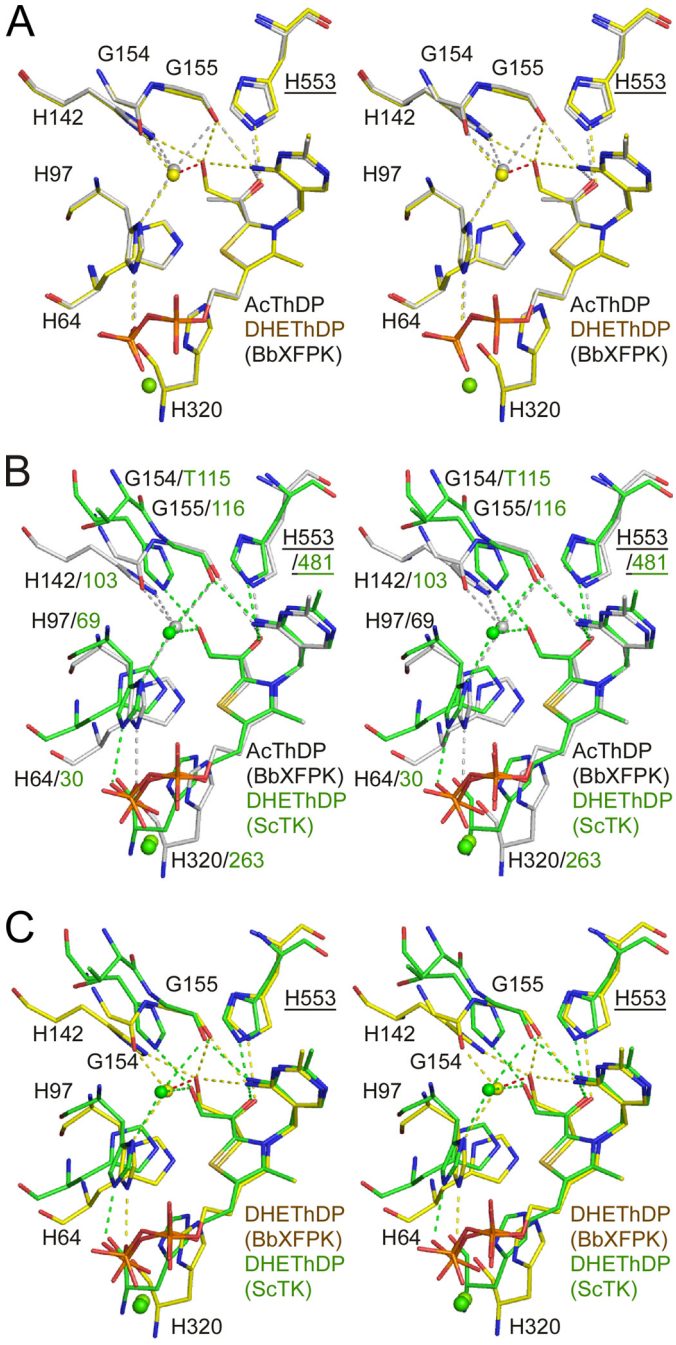

FIGURE 5. **Stereo view of superimposed structures of covalent ThDP adducts in *Bb*XFPK and *Sc*TK.** Superimposition of AcThDP (*gray*) and DHEThDP (*yellow*) in *Bb*XFPK (*A*), AcThDP in *Bb*XFPK (*gray*) and DHEThDP in *Sc*TK (*green*) (*B*), and DHEThDP in *Bb*XFPK (*yellow*) and *Sc*TK (*green*) (*C*). Labels for residues from the Pyr domain of the other subunit are *underlined*. The water molecules near the covalent adducts are shown as *spheres*.

3.2 Å from the terminal Cβ atom of the acetyl group (discussed later).

Then we prepared a crystal by soaking in 54 mM F6P for a short time period (15 s), and a clear electron density peak corresponding to the Cβ hydroxyl group of DHEThDP was observed (Fig. 4*C*). The electron density map for the DHE moiety is relatively weak but is sufficiently clear in shape, and is interpreted as DHEThDP. An electron density peak that corresponds to the water molecule in the AcThDP structure

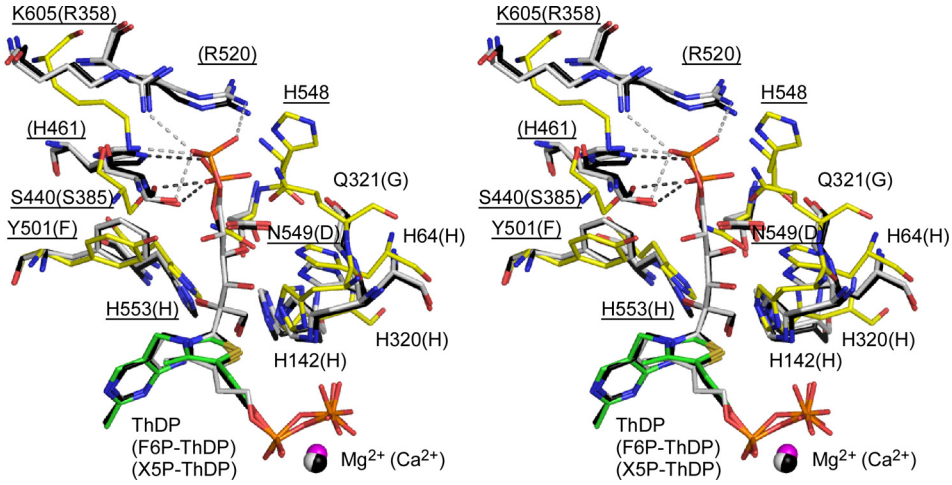

FIGURE 6. **Stereo view of superimposition between *Bb*XFPK and tetrahedral donor substrate adducts of *Ec*TK.** Resting *Bb*XFPK (*yellow* for protein and *green* for cofactor), X5P-ThDP (2R8O, *black*), and F6P-ThDP adduct of *Ec*TK (2R8P, *gray*) are shown. Residues expected to participate in F6P binding are shown as *stick models*. *Labels in parentheses* are those of *Ec*TK.

was also observed, but the distance from the Cβ hydroxyl atom (Oβ) was abnormally close (2.0 Å). We repeatedly refined the crystal structure by changing the occupancies of these elements (the DHE moiety and the water molecule) and then examined the resultant $|F_o| - |F_c|$ difference map. We finished the refinement by setting the occupancies to 0.7 for the water molecule (B factor = 9.8 Å^2), 0.3 for the Oβ atom (B factor = 16.3 Å^2), and 0.5 for the other three atoms of the DHE moiety (Cα, Oα, and Cβ; average B factor = 24.9 Å^2). The average B factor of the remaining moiety of the ThDP cofactor was 18.8 Å^2. Thus, this crystal was assumed to be a mixture of free ThDP with the water (0.5 fraction), DHEThDP without the water (0.3), and AcThDP with the water (0.2). This result indicates that the DHEThDP intermediate is transient under this condition. The map around the central Cα atom is not planar, suggesting that this atom has an sp^3-hybridized character (Fig. 4*C*, *inset*). Because of limited resolution (2.1 Å), low occupancy (0.3), and the electron density overlaps with those of other states, the hybridization state of the Cα atom cannot be determined unambiguously. However, crystallographic refinement with parameters of the sp^2 hybridized (flat) Cα atom resulted in the appearance of significant difference peaks near the Oα and Oβ atoms in the $|F_o| - |F_c|$ map (data not shown). Observation of the sp^3-hybridized Cα atom suggests that the resonance hybrid between the neutral enamine and zwitterionic α-carbanion in our DHEThDP structure is unlikely present. Instead, the structure is likely a protonated state at the Cα atom with the *S*-configuration (*S*-α,β-dihydroxyethyl-ThDP; Fig. 2, *boxed with a broken line*). Although the crystal structure was obtained at pH 9.0, the local environment may stabilize the protonated state. In contrast, the DHEThDP intermediate of *Sc*TK was observed as an sp^2-hybridized enamine character (Fig. 5*C*) (4). The terminal Cβ hydroxyl group interacts with the NE2 atom of His-142 (2.9 Å), the main chain oxygen atom of Gly-155 (2.9 Å), and the N4′ group of the pyrimidine moiety (3.2 Å). The branched Cα hydroxyl group interacts with the NE2 atom of His-553 (2.6 Å), but the N4′ atom of pyrimidine moiety is distant (3.6 Å).

The fourth structure, a complex with the acceptor substrate, P_i, was prepared by cocrystallization in the presence of P_i. A clear tetrahedral electron density peak was observed near the C2 atom of the thiazolium ring (Fig. 4*D*). The four structures of the wild-type *Bb*XFPK determined in this work did not show any significant conformational changes around the active site. This observation indicates that the formation of reaction intermediates and binding of the acceptor substrate do not induce remarkable conformational change, which is consistent with previous findings in *Sc*TK (4) and *Lp*POX (34).

Substrate Binding Channel of BbXFPK—The substrate binding channel of *Sc*TK has been identified by the complex structure with erythrose 4-phosphate (35). Moreover, the crystal structures of TK from *E. coli* (*Ec*TK) in complex with uncleaved donor substrates, tetrahedral covalent X5P-ThDP and F6P-ThDP adducts, have been reported (36). In the tetrahedral substrate-cofactor adducts, the C2-Cα bond between the cofactor and substrate is distorted from the planarity, and the leaving group is perpendicularly orientated to the thiazolium ring of ThDP (Fig. 6). The out-of-plane distortions of the C2-Cα bond and the perpendicular orientation of the leaving groups are considered to facilitate the elimination of the first product (9, 37). Therefore, the covalent F6P-ThDP adduct of *Bb*XFPK is also expected to adopt a similar conformation. Superimposition of the resting *Bb*XFPK and F6P-ThDP adduct of *Ec*TK revealed that F6P can bind in the active site channel of *Bb*XFPK without any steric hindrance, leading to the estimation of residues involved in substrate recognition (Fig. 6). To verify the importance of these residues in substrate recognition and catalysis, we constructed mutants of residues located in this site (His-64, His-142, His-320, Gln-321, Ser-440, His-548, Asn-549, and His-553) (Table 2). The His residues near the sugar-derived hydroxyl groups (His-64, His-142, His-320, and His-553) are completely conserved, and mutation of these residues significantly impaired the activity (discussed later). In *Ec*TK, Arg-358, Arg-520, His-461, and Ser-385 recognize the distal phosphate group of F6P. In the X5P-ThDP adduct, the phosphate is slightly displaced, and the hydrogen bonds with Arg-358 and Arg-520 disappear. In the *Bb*XFPK structure, only Ser-440 is conserved, but additional residues (His-548, Gln-321, and Asn-549) appear to strengthen the interactions. Mutation of these residues also significantly impaired the activity (Table 2). We expected the presence of a distinct residue conservation pattern between the XPK and XFPK groups around this region. However, the directly interacting residues are completely conserved (supplemental Fig. 1*A*), and we could not find any significant pattern that can predict the substrate preference to X5P and F6P. Surrounding residues that do not directly interact with the substrate may be responsible for the substrate specificity. As

shown in supplemental Table 1, the substrate preferences of XFPK and XPK groups are not very significant. The XPK-type enzyme from *L. plantarum* prefers X5P to F6P, but the V_{max}/K_m ratio is only about 15.

Dehydration Mechanism—Observation of the DHEThDP and AcThDP adducts after soaking the crystals in F6P for very short and relatively long periods of time, respectively, supports the previous notion that the dehydration occurs in the absence of P_i (22, 33). The water molecule observed near AcThDP is held by four hydrogen bonds with the side chain N atoms of His-97 and His-142 and the main chain O atoms of Gly-154 and Gly-155 (Fig. 5*A*). The water molecule is slightly displaced in the DHEThDP structure, and the hydrogen bonds with His-142 and Gly-155 are disengaged. This site appears to be suitable for occupation by the water molecule derived from the dehydration reaction. A similar water binding site is present in *Sc*TK, although TK does not catalyze dehydration (Fig. 5, *B* and *C*). The water molecule in *Sc*TK is located at a significantly distant position from the Cβ hydroxyl group of DHE (3.0 Å) compared with that in *Bb*XFPK. The Thr-115 residue in *Sc*TK corresponding to Gly-154 in *Bb*XFPK is significantly displaced because of the difference in the main chain trace, and hence, there is no hydrogen bond to the water molecule.

In a possible reaction mechanism of PK, a proton acceptor (B_1) is required to deprotonate the C3 hydroxyl group of the tetrahedral donor substrate-ThDP adduct for the elimination of the first product (Fig. 2). The candidates for the B_1 catalyst, His-64 and His-320 of *Bb*XFPK, are positioned close to the C3 hydroxyl group of F6P-ThDP (Fig. 6). The subsequent dehydration reaction requires a proton donor (B_2) to protonate the C1 hydroxyl group leaving from DHEThDP (Fig. 2). The candidates for the B_2 catalyst, His-142 (2.9 Å), His-553 (3.4 Å), and the N4′ group of the pyrimidine moiety (3.2 Å), are positioned close to the Cβ hydroxyl group of DHEThDP (Fig. 5*A*). These His residues (His-64, His-142, His-320, and His-553) are completely conserved in all PKs (supplemental Fig. 2). Mutations of these residues completely abolished the activity except in H142A and H142N (Table 2). We also performed crystallographic analysis of H64A, H142A, H320A, and H553A mutants because the tetrahedral F6P-ThDP or DHEThDP intermediates were expected to be trapped in the B_1 and B_2 catalyst mutants, respectively (Fig. 2). The electron density maps of the data collected from crystals of these mutants soaked in 27 mM F6P for 5 min are shown in Fig. 4*E* and supplemental Fig. 4. As summarized in Table 2, we could not obtain any of these expected intermediates; only adduct-free ThDP (H64A and H553A) or AcThDP (H142A and H320A) were observed. The ThDP cofactor in H64A was in a unique tricyclic ring form (discussed below). Based on these results, His-142 and His-320 are excluded from the candidates of B_1 and B_2 catalysts. Although the DHEThDP intermediate was not observed in the H64A structure, His-64 is a better candidate for the B_1 catalyst than His-320. In the case of *Sc*TK, the His-64 counterpart (His-30) and the His-320 counterpart (His-263) are thought to act in concert during the catalytic step, but the latter has been assigned to be the B_1 catalyst (3, 38). His-553 and the N4′ group of the pyrimidine moiety are possible B_2 candidate, but the latter cannot be investigated by a mutational method. If His-553 is the B_2 catalyst, the reason why an adduct-free ThDP is trapped by the H553A mutation is unclear. This residue may also be important for the preceding steps of dehydration. For example, His-553 seems to stabilize the tetrahedral donor substrate-ThDP adduct by forming an interaction with the C2 hydroxyl group (Fig. 6). In the case of *Sc*TK, the His-553 counterpart (His-481) is thought to stabilize the transition state of the step catalyzed by B_1 (38). Another candidate for the B_2 catalyst is His-97 (Fig. 5*A*). His-97 is located at a relatively distant position from the Cβ hydroxyl group of DHEThDP (4.2 Å) but sufficiently close to the water molecule near AcThDP. As shown in Table 2, H97A and H97N mutants showed no catalytic activity. We tried to determine their structures in the presence of F6P but failed due to poor reproducibility of crystallization. This may be because this residue is also involved in fixation of the diphosphate moiety of ThDP (Fig. 5).

Structure of a Tricyclic Ring Form of ThDP—To our surprise, in the electron density map of the H64A mutant, the N4′ atom of the pyrimidine ring and the C2 atom of the thiazolium ring were close to each other and within covalent bonding distance, exhibiting a tricyclic character (Fig. 4*E*). Furthermore, this tricyclic ring thiamine cofactor was observed from crystals of H64A mutants without soaking in F6P (data not shown). The central ring is six-membered and is clearly different from the shape of a carbinolamine form, which has a seven-membered central ring formed by a covalent bond between the carbonyl carbon of a substituted acetyl group on the C2 atom of the thiazolium ring and the N4′ atom of the pyrimidine ring (34, 39). The cofactor derivative was, instead, interpreted as a tricyclic form observed in the active site of acetolactate synthase (40). The electron density map was reasonably fit with a pyramidal N3 atom because the thiazolium and central rings form an acute angle. The effect of deleting the side chain of His-64 appears to propagate to another subunit, and a region holding the pyrimidine and thiazolium rings is significantly displaced toward the outside of subunit interface (supplemental Fig. 5). As a result, the pocket for the cofactor rings is relatively open in the H64A mutant and provides flexibility. The flexibility might have permitted migration of the positive charge from N3 to S1 to facilitate the tricyclic ring formation as in the case of acetolactate synthase (40). It is also possible that x-ray radiation damage caused the cyclization. The drastic reduction in the catalytic activity of H64A is attributed to the inactivation of the cofactor by the significant change of its form. Therefore, the abovementioned possibility that His-64 works as the B_1 catalyst is not ruled out.

Nucleophilic Attack on AcThDP by P_i—The P_i binding site of *Bb*XFPK is formed by His-64, His-320, Gln-321, Tyr-501, and Asn-549 (Fig. 7*A*). Mutations of these residues dramatically decreased the activity (Table 2). In particular, replacement of Tyr-501 by phenylalanine significantly elevated the K_m value for P_i. The residue corresponding to Tyr-501 is generally Phe in TKs (Phe-442 in *Sc*TK). The distance between an oxygen atom of P_i and the Cα carbon of AcThDP is 3.1 Å, and the O(Pi)···Cα—Oα angle is 115° (Fig. 7*A*). This spatial configuration is within the limits of the Bürgi-Dunitz trajectory (41), suggesting that the nucleophilic attack by the acceptor substrate (P_i) occurs on the keto form and not on the enol form

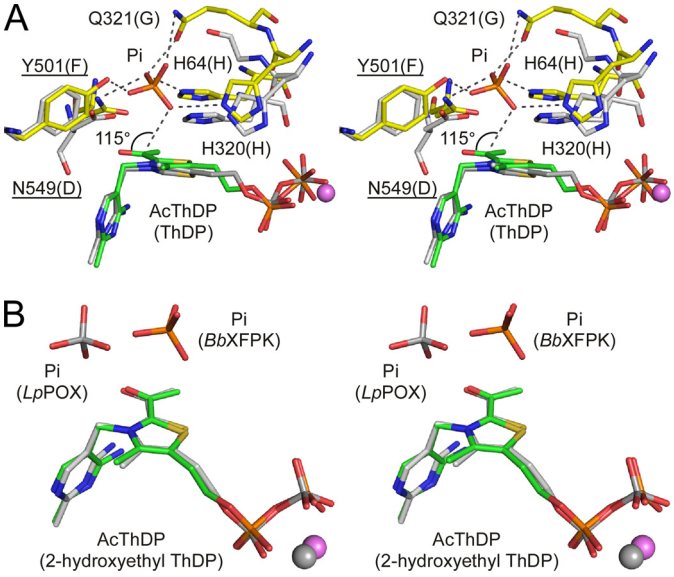

FIGURE 7. **Stereo view of superimposition of the P_i binding site of *Bb*XFPK with *Sc*TK (*A*) and *Lp*POX (*B*).** *A*, shown is superimposition of the AcThDP and P_i complex structures of *Bb*XFPK (*yellow* for protein and *green* for cofactor) and the resting structure of *Sc*TK (PDB code 1TRK, *gray*). *Labels in parentheses* are those of *Sc*TK. *B*, shown is superimposition of the AcThDP intermediate and P_i complex structures of *Bb*XFPK (C and P atoms are in *green* and *orange*, respectively), and P_i complexed with α-hydroxyethyl-ThDP adduct of *Lp*LOX (2EZT, C and P atoms are in *gray*).

(Fig. 2). In contrast, the nucleophilic attack in TK is reversely performed by the α-carbanion DHEThDP on the acceptor substrate (aldose in this case).

This part of the reaction of *Bb*XFPK is analogous to that of acetyl-P-producing POX, which also produces acetyl-P after nucleophilic attack by P_i (9, 34, 42). However, the reaction of POX is distinct from that of PK because the nucleophilic attack occurs on the radical state of AcThDP (or 2-hydroxyethyl-ThDP) and involves electron transfer to a flavin adenine dinucleotide cofactor. The P_i molecule bound to the α-hydroxyethyl-ThDP adduct of *Lp*POX is also located in the vicinity of the Cα atom of the covalent adduct, but its spatial configuration is different from that of *Bb*XFPK (Fig. 7*B*).

DISCUSSION

Our study expanded the structural insight into the reaction mechanism of PK. The reaction of PK is distinct from that of other ThDP-dependent enzymes at the point of dehydration. In this study we trapped the structures of two key intermediates before and after dehydration and showed that AcThDP accumulates in the absence of P_i as a stable intermediate. However, the identity of the critical factor for dehydration that discriminates PK from TK remains to be determined. An ^{1}H NMR study has shown that AcThDP does not form in the active site of TK (43), indicating that the TK reaction is completely devoid of dehydration. Mutagenesis and crystallographic analysis of *Bb*XFPK indicated that the most probable candidate for the B_1 catalyst is His-64. Identity of the B_2 catalyst remains elusive, but possible factors responsible for the dehydration step are assigned to be His-553, the N4′ group of the pyrimidine, or His-97. It is confusing that there is no clear structural difference from TK in the catalytic center region around the Cβ hydroxyl group of DHEThDP. However, the environment around the water molecule observed near the AcThDP adduct seems to be critical for the dehydration reaction. This reaction is elimination of a hydroxyl group from an enamine tautomer catalyzed by a catalytic acid. The dehydration reaction of PK is analogous to the second β-elimination step of the dehydration reaction catalyzed by enolase, which is involved in major glycolytic pathways (44). Observation of the tricyclic ring form of ThDP in the active site of *Bb*XFPK is noteworthy, as this form is not usually observed in ThDP-dependent enzymes. Unlike the case of ALS, a point mutation resulted in the formation of this unique but catalytically inactive form of the cofactor.

Acknowledgment—We thank the staff of the Photon Factory and SPring-8 for the X-ray data collection.

Note Added in Proof—The crystal structure of XFPK from *B. longum* is reported by Takahashi *et al.* (Takahashi, K., Tagami, U., Shimba, N., Kashiwagi, T., Ishikawa, K., and Suzuki, E. (2010) *FEBS Lett.* **584,** 3855–3861).

REFERENCES

1. Guarner, F., and Malagelada, J. R. (2003) *Lancet* **361,** 512–519
2. Scardovi, V., and Trovatelli, L. D. (1965) *Ann. Microbiol.* **15,** 19–29
3. Schneider, G., and Lindqvist, Y. (1998) *Biochim. Biophys. Acta* **1385,** 387–398
4. Fiedler, E., Thorell, S., Sandalova, T., Golbik, R., König, S., and Schneider, G. (2002) *Proc. Natl. Acad. Sci. U.S.A.* **99,** 591–595
5. Heath, E. C., Hurwitz, J., Horecker, B. L., and Ginsburg, A. (1958) *J. Biol. Chem.* **231,** 1009–1029
6. Hurwitz, J. (1958) *Biochim. Biophys. Acta.* **28,** 599–602
7. Schramm, M., Klybas, V., and Racker, E. (1958) *J. Biol. Chem.* **233,** 1283–1288
8. Breslow, R. (1958) *J. Am. Chem. Soc.* **80,** 3719–3726
9. Kluger, R., and Tittmann, K. (2008) *Chem. Rev.* **108,** 1797–1833
10. Duggleby, R. G. (2006) *Acc. Chem. Res.* **39,** 550–557
11. Jordan, F. (2003) *Nat. Prod. Rep.* **20,** 184–201
12. Tittmann, K. (2009) *FEBS J.* **276,** 2454–2468
13. Muller, Y. A., and Schulz, G. E. (1993) *Science* **259,** 965–967
14. Goldberg, M. L., and Racker, E. (1962) *J. Biol. Chem.* **237,** 3841–3842
15. Sgorbati, B., Lenaz, G., and Casalicchio, F. (1976) *Antonie Van Leeuwenhoek* **42,** 49–57
16. Meile, L., Rohr, L. M., Geissmann, T. A., Herensperger, M., and Teuber, M. (2001) *J. Bacteriol.* **183,** 2929–2936
17. Sánchez, B., Zúñiga, M., González-Candelas, F., de los Reyes-Gavilán, C. G., and Margolles, A. (2010) *J. Mol. Microbiol. Biotechnol.* **18,** 37–51
18. Scardovi, V. (1986) in *Bergey's Manual of Systematic Bacteriology* (Sneath, P. H. A., Mair, N. S., Sharpe, M. E., and Holt, J. G., eds) pp 1418–1434, Williams and Wilkins, Baltimore
19. Vlková, E., Nevoral, J., Jencikova, B., Kopecný, J., Godefrooij, J., Trojanová, I., and Rada, V. (2005) *J. Microbiol. Methods.* **60,** 365–373
20. Panagiotou, G., Andersen, M. R., Grotkjaer, T., Regueira, T. B., Hofmann, G., Nielsen, J., and Olsson, L. (2008) *PloS one.* **3,** e3847
21. Maslowski, K. M., Vieira, A. T., Ng, A., Kranich, J., Sierro, F., Yu, D., Schilter, H. C., Rolph, M. S., Mackay, F., Artis, D., Xavier, R. J., Teixeira, M. M., and Mackay, C. R. (2009) *Nature* **461,** 1282–1286
22. Yevenes, A., and Frey, P. A. (2008) *Bioorg Chem.* **36,** 121–127
23. Petrareanu, G., Balasu, M. C., Zander, U., Scheidig, A. J., and Szedlacsek, S. E. (2010) *Acta Crystallogr. Sect. F Struct. Biol. Cryst. Commun.* **66,** 805–807
24. Suzuki, R., Kim, B.-J., Iwamoto, Y., Katayama, T., Ashida, H., Wakagi, T., Shoun, H., Fushinobu, S., and Yamamoto, K. (2010) *Acta Crystallogr. Sect. F Struct. Biol. Cryst. Commun.* **66,** 941–943
25. Otwinowski, Z., and Minor, W. (1997) *Methods Enzymol.* **276,** 307–326
26. Rappleye, J., Innus, M., Weeks, C. M., and Miller, R. (2002) *J. Appl. Crys-*

tallogr **35,** 374–376
27. Terwilliger, T. C., and Berendzen, J. (1999) *Acta. Crystallogr. D Biol. Crystallogr.* **55,** 849–861
28. Perrakis, A., Morris, R., and Lamzin, V. S. (1999) *Nat. Struct. Biol.* **6,** 458–463
29. Emsley, P., and Cowtan, K. (2004) *Acta Crystallogr. D Biol. Crystallogr.* **60,** 2126–2132
30. Murshudov, G. N., Vagin, A. A., and Dodson, E. J. (1997) *Acta. Crystallogr. D Biol. Crystallogr.* **53,** 240–255
31. Schüttelkopf, A. W., and van Aalten, D. M. (2004) *Acta. Crystallogr. D Biol. Crystallogr.* **60,** 1355–1363
32. Kern, D., Kern, G., Neef, H., Tittmann, K., Killenberg-Jabs, M., Wikner, C., Schneider, G., and Hübner, G. (1997) *Science* **275,** 67–70
33. Frey, P. A. (1989) *Biofactors* **2,** 1–9
34. Wille, G., Meyer, D., Steinmetz, A., Hinze, E., Golbik, R., and Tittmann, K. (2006) *Nat. Chem. Biol.* **2,** 324–328
35. Nilsson, U., Meshalkina, L., Lindqvist, Y., and Schneider, G. (1997) *J. Biol. Chem.* **272,** 1864–1869
36. Asztalos, P., Parthier, C., Golbik, R., Kleinschmidt, M., Hübner, G., Weiss, M. S., Friedemann, R., Wille, G., and Tittmann, K. (2007) *Biochemistry* **46,** 12037–12052
37. Tittmann, K., and Wille, G. (2009) *J. Mol. Catal. B Enzym.* **61,** 93–99
38. Wikner, C., Nilsson, U., Meshalkina, L., Udekwu, C., Lindqvist, Y., and Schneider, G. (1997) *Biochemistry* **36,** 15643–15649
39. Gruys, K. J., Halkides, C. J., and Frey, P. A. (1987) *Biochemistry* **26,** 7575–7585
40. Pang, S. S., Duggleby, R. G., Schowen, R. L., and Guddat, L. W. (2004) *J. Biol. Chem.* **279,** 2242–2253
41. Bürgi, H. B., and Dunitz, J. D. (1983) *Acc. Chem. Res.* **16,** 153–161
42. Tittmann, K., Wille, G., Golbik, R., Weidner, A., Ghisla, S., and Hübner, G. (2005) *Biochemistry* **44,** 13291–13303
43. Tittmann, K., Golbik, R., Uhlemann, K., Khailova, L., Schneider, G., Patel, M., Jordan, F., Chipman, D. M., Duggleby, R. G., and Hübner, G. (2003) *Biochemistry* **42,** 7885–7891
44. Reed, G. H., Poyner, R. R., Larsen, T. M., Wedekind, J. E., and Rayment, I. (1996) *Curr. Opin. Struct. Biol.* **6,** 736–743
45. Lovell, S. C., Davis, I. W., Arendall, W. B., 3rd, de Bakker, P. I., Word, J. M., Prisant, M. G., Richardson, J. S., and Richardson, D. C. (2003) *Proteins* **50,** 437–450